

Electrical trace analysis of superconducting nanowire photon-number-resolving detectors

Timon Schapeler^{1,2,*}, Niklas Lamberty¹, Thomas Hummel¹, Fabian Schlue¹, Michael Stefszky³, Benjamin Brecht³, Christine Silberhorn³ and Tim J. Bartley^{1,2}

¹*Department of Physics, Paderborn University, Warburger Strasse 100, Paderborn 33098, Germany*

²*Institute for Photonic Quantum Systems (PhoQS), Paderborn University, Warburger Strasse 100, Paderborn 33098, Germany*

³*Integrated Quantum Optics Group, Institute for Photonic Quantum Systems (PhoQS), Paderborn University, Warburger Strasse 100, Paderborn 33098, Germany*

(Received 10 November 2023; revised 7 February 2024; accepted 17 May 2024; published 10 July 2024)

We apply principal component analysis (PCA) to a set of electrical output signals from a commercially available superconducting nanowire single-photon detector (SNSPD) to investigate their photon-number-resolving capability. We find that the rising edge as well as the amplitude of the electrical signal have the most dependence on photon number. Accurately measuring the rising edge while simultaneously measuring the voltage of the pulse amplitude maximizes the photon-number resolution of SNSPDs. Using an optimal basis of principal components, we show unambiguous discrimination between one- and two-photon events, as well as partial resolution up to five photons. This expands the use case of SNSPDs to photon-counting experiments, without the need of detector multiplexing architectures.

DOI: [10.1103/PhysRevApplied.22.014024](https://doi.org/10.1103/PhysRevApplied.22.014024)

I. INTRODUCTION

The ability to count photons is desirable in a great many quantum optics experiments and applications, not least quantum computing paradigms [1], quantum communication [2,3], and multiphoton metrology [4]. While some energy-resolving detectors function at the single-photon level, they are often slow devices with limited timing resolution [5]. Instead, single-photon detectors, which detect the presence or absence of photons but cannot resolve the photon number, can offer quasi-photon-number resolution when configured in multiplexing architectures [6–12] or array readout design [13–18]. Within this class of detectors, superconducting nanowire single-photon detectors (SNSPDs) have become the gold standard due their unmatched signal-to-noise ratio [19] and high timing resolution [20].

While long regarded as a threshold detector, careful analysis of the detector signal has recently demonstrated that they also show limited photon-number information in

their electrical output signal. The first evidence of photon-number resolution using an SNSPD has been presented by Cahall *et al.* [21] and was attributed to a time- and photon-number-dependent hot-spot resistance of the nanowire. By investigating the different rise times from the electrical output signal of the detector, the authors show evidence up to four-photon detection events. These findings are consistent with a generalized electrothermal model [22] based on Ref. [23]. This model links hot-spot growth and the rising edge of the electrical output signal of the detector. Another approach to gain photon-number resolution from SNSPDs has been presented by Zhu *et al.* [24], where the amplitude of the detector output signal directly correlates with the photon number up to five photons. This has been achieved by combining a single superconducting nanowire with an impedance-matching taper, which makes the amplitude of the output signal sensitive to the number of hot spots induced by absorbed photons, as predicted by Bell *et al.* [25]. Further, in an attempt to be more resistant against noise, Endo *et al.* have used an oscilloscope to record reference wave forms corresponding to different photon numbers, which could then be used to distinguish different events by wave-form pattern matching. They have found that using a subset of the rising edge of the SNSPD output trace improves the photon-number discrimination for larger input states, compared to merely using a single point in time [26]. Alternative approaches for photon-number resolution involve analyzing the rising

*Corresponding author: timon.schapeler@upb.de

edge of the output signal. One method utilizes a linear fit to a section of the rising edge, with the photon number determined from the corresponding slope measured using an oscilloscope [27]. Another method measures the variation in the slew rate of the SNSPD output signal, employing a constant-threshold time tagger to determine the difference in arrival time of detection events relative to a trigger signal [28].

The most recent method to resolve photon number with a single SNSPD builds on this idea and measures the relative time difference between a trigger signal and the rising and falling edges of the electrical detector output signal, which enhances the discrimination of different photon numbers [29].

While investigating the full electrical output signal of a detector maximizes the amount of information from a detection event, this is not practical in experiments where photon-number information must be extracted in real time. The question naturally arises: which aspects of the electrical output provide most information about the photon number? To answer this question, in this paper we use a popular technique from multivariate statistics known as principal component analysis (PCA) [30] to deduce maximum information about the photon number from a minimum number of data points.

In general, PCA is a dimensionality-reduction technique that determines a set of optimal orthogonal basis functions (principal components) describing the maximum amount of information in a data set. That means that it transforms the data set, containing lots of variables, into a smaller data set, being less accurate but with reduced complexity. This is done by calculating the covariance matrix of the data set and finding the eigenvectors of the largest eigenvalues of the covariance matrix. The eigenvectors (also called principal components in PCA terms) correspond to the directions of maximum variance, i.e., information in the data set. PCA has already been applied to the electrical output signals from transition-edge sensors (TESs) [31], where it has been successfully used to reduce the complexity of the data set by focusing on the first principal components.

In this work, we make use of the full electrical output signal of the commercially available SNSPD, maximizing the amount of information from any detection event. From this, we will use PCA to investigate the extent to which SNSPDs can resolve the photon number and to identify which features of the electrical output signal are most relevant for maximizing the photon-number-resolving capability. Following that, we make use of the knowledge from the PCA and use a time tagger to verify our findings. We use a more application-oriented method of recording the relative time differences between a trigger signal and the rising and falling edges of the SNSPD electrical output signal [29].

As this method relies on a trigger signal to gain photon-number information, pulsed light is necessary. Previous

methods [21,24,27] do not rely on a trigger signal and could thus be used for continuous-wave light. However, to have significant multiphoton components in the short time window, where the photon-number-resolving detection mechanism works (up to tens of picoseconds [32]), the photon flux would cause the SNSPDs to latch. We investigate a single-pixel SNSPD, to show the photon-number-resolving capability of just one pixel. However, this method can also be applied to SNSPD arrays, where each pixel is read out individually [10,12], to further increase the photon-number resolution of these arrays.

II. EXPERIMENTAL SETUP

The experiment consists of recording the electrical output signal from a commercially available SNSPD with an oscilloscope. The experimental setup can be seen in Fig. 1. We use a < 200-fs pulsed laser, as recent theoretical simulations suggest that longer delays between absorbed photons decrease resolvability [32]. After taking fiber dispersion into account, the temporal pulse width is approximately 3 ps at the detector. Since the SNSPD cannot be operated at the repetition rate of the pulsed laser of 80 MHz, we pick every 800th pulse to reduce the repetition rate to 100 kHz. This is done by dividing the synchronization output of the laser with a pulse divider, which is then used as a trigger for an arbitrary wave-form generator (AWG) to generate a 8.3-ns pulse for the pulse-picking electro-optic modulator (EOM). We use a power supply to set a dc offset voltage to the EOM, in order to optimize the extinction ratio of the pulse-picking system. The polarization controller before and the fiber polarizing beam splitter (PBS) after the EOM are used to optimize the polarization of the light toward the SNSPD. One port of the PBS is connected to a fiber attenuator (in order to attenuate the light close to the single-photon level) and two variable optical attenuators (VOA) control the precise mean photon number impinging on the detector. The second polarization controller is used to optimize the detection efficiency of the polarization-dependent SNSPD. The second port of the fiber PBS is connected to a fast photodiode (1.2-GHz bandwidth), which acts as a trigger for the oscilloscope. We use a 21-GHz-bandwidth oscilloscope with 128 GSa/s to record the electrical signal of the SNSPD. This gives us a sampling period of roughly 8 ps, while maintaining the full information of the electrical signal of the detector. The commercially available SNSPD has a timing jitter of 11.3 ps (FWHM), specified by the manufacturer (Single Quantum).

The oscilloscope is operated in a sequential acquisition mode, where 1000 electrical output traces are recorded at once and then streamed to a computer. One trace consists of 3×10^4 points, which corresponds to a length in time of approximately 234 ns. We scan through mean photon numbers from 0.5 to 5 in steps of 0.5 and record 1×10^5 traces

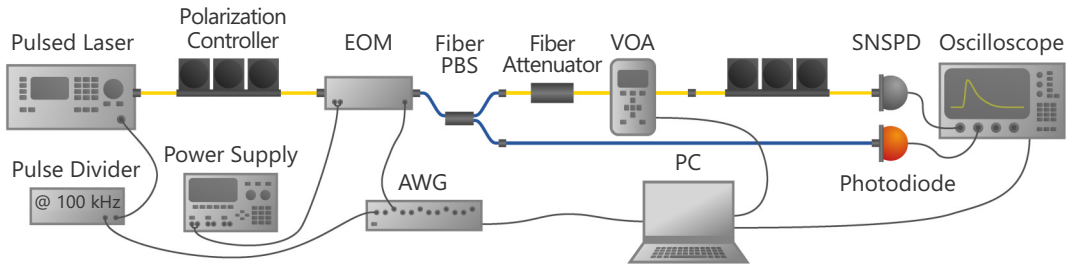


FIG. 1. We use a femtosecond-pulsed laser at 80 MHz, which is pulse-picked down to 100 kHz using an electro-optic modulator (EOM). The EOM receives a square-wave function from an arbitrary wave-form generator (AWG) and a dc offset voltage from a power supply. The polarization controller and the fiber polarizing beam splitter (PBS) are used to optimize the optical power incident on the SNSPD. A fiber attenuator and a variable optical attenuator are used to attenuate the laser light and set different mean photon numbers. The second polarization controller is used to optimize the signal on the SNSPD. The second port of the fiber PBS is connected to a fast photodiode, which is used as the trigger for the oscilloscope. The yellow and blue fibers represent single-mode and polarization-maintaining fiber, respectively.

per mean photon number. An exception is the mean photon number of 0.5, for which we record twice as many traces, since a lot of pulses contain zero photons. Every instance of zero impinging photons results in an empty trace, which contains no relevant information for the PCA. We randomize the order of the 1100 measurements, to avoid any bias toward photon number that might occur due to possible drifts during the measurement.

In a second measurement, we substitute the oscilloscope for a time tagger with a time resolution of < 1.9 ps. This measurement is used to confirm our findings of the subsequent PCA method, in order to maximize the photon-number-resolving capability of the commercial SNSPD using a time tagger.

The mean photon numbers as a function of attenuation are calibrated before the measurement. This is done by recording the count rate (r_{count}) of the SNSPD over the full operating range [from dark counts until saturation, where the count rate equals the repetition rate (r_{rep}) of the experiment] with a time tagger, by sweeping the attenuation using the VOAs. Assuming Poissonian statistics of the laser, the mean detected photon number per pulse is then given by

$$\bar{n} = -\ln \left(1 - \frac{r_{\text{count}}}{r_{\text{rep}}} \right). \quad (1)$$

III. RESULTS

The full data set of electrical output signals consists of 1.1×10^6 traces (also called samples) and 3×10^4 points per trace, i.e., time-dependent voltages (also called features). However, we only use 1.9×10^4 points, as this is enough to contain the complete SNSPD electrical trace. In a first step, we filter out traces from suboptimal pulse picking (i.e., traces with multiple peaks or traces at the wrong time delay with respect to the trigger signal) as well as empty traces (when no photon was detected, after

the trigger signal from the fast photodiode). This means that in the PCA we will not investigate the zero-photon (vacuum) component of the coherent state, as we want to investigate the photon-number-resolving capability of the detector. Since the discrimination of click and no-click events is trivial, we focus only on the click events (at least one photon).

As a next step, we fit the PCA model with a subset of 1000 samples from each mean photon number (using more samples did not change the fit). This yields the principal components f_1 and f_2 in Fig. 2, which describe the most information of the data set (we show covariance matrices in Fig. 6). The model is then successively applied to the full data set in order to find the weights corresponding to the principal components for each sample. From our analysis, we find that only the first two principal components show photon-number dependency. Plotting the weights of the first component against the weights of the second component in a two-dimensional histogram shows a clear

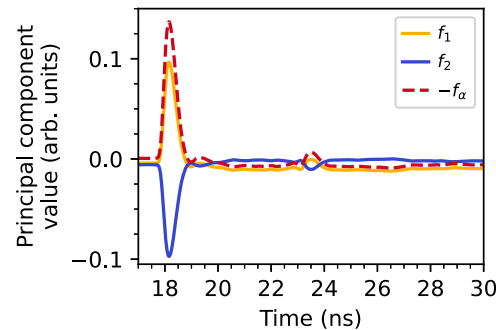


FIG. 2. First two principal components (basis functions), f_1 and f_2 , and the principal component that results from the optimal angle projection $-f_\alpha$ of the two-dimensional histogram in Fig. 3(a). Only the relevant time regime is shown; the basis functions are flat otherwise.

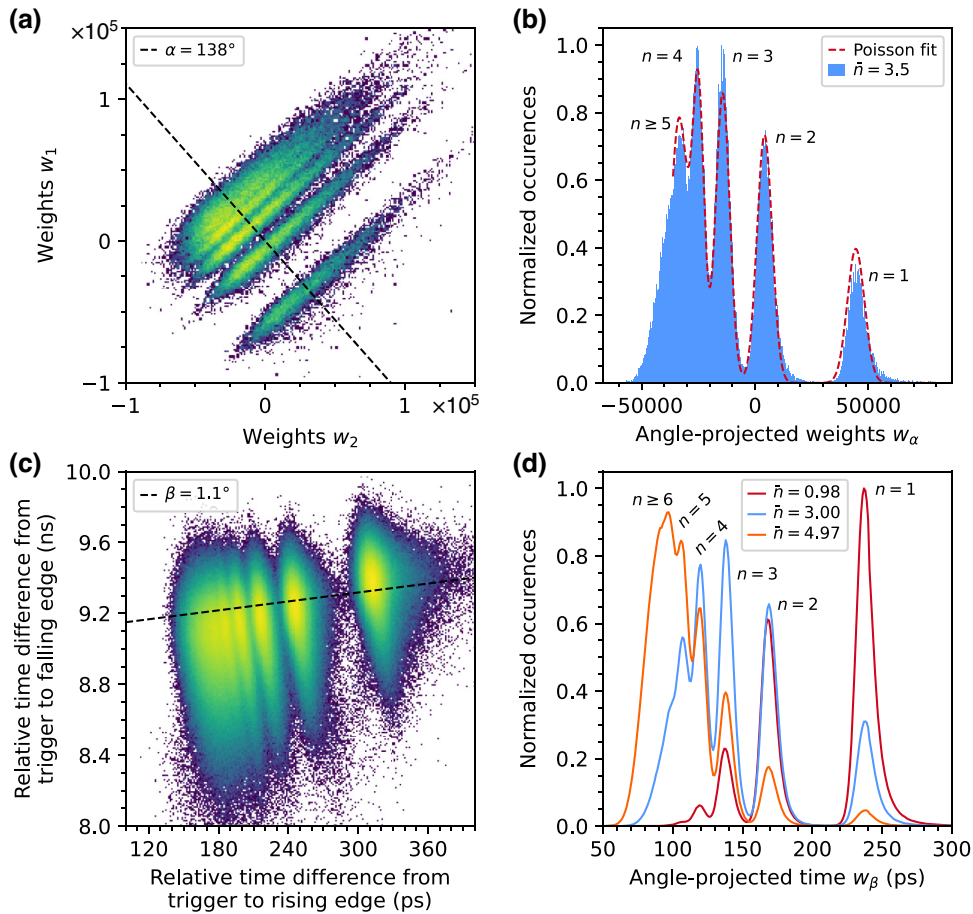


FIG. 3. (a) The two-dimensional histogram of the weights of the first two principal components from the PCA model for a mean photon number of $\bar{n} = 3.5$. These two components show a photon-number dependency, which can be seen by the clear differentiation between the ellipses. For smaller mean photon numbers, the occupation of the ellipses shifts to the lower right and for higher mean photon numbers to the upper left. (b) The histogram of the optimal projection at an angle of $\alpha = 138^\circ$ and a multi-Gaussian fit with an enforced Poisson distribution (red dashed line). Additional two-dimensional histograms and their optimal projection (for mean photon numbers of $\bar{n} = 1$, $\bar{n} = 3$, and $\bar{n} = 5$) are shown in Fig. 7. (c) The two-dimensional histogram of the relative time difference between the trigger signal and the rising and falling edge. The full data set is displayed, which is the sum of the individual measurements for the three mean photon numbers indicated in (d). (d) The optimal projection at an angle of $\beta = 1.1^\circ$ of the two-dimensional histogram of (c) for three photon numbers (as labeled in the legend).

differentiation between photon numbers [see Fig. 3(a), where the mean photon number is $\bar{n} = 3.5$].

Due to the angle of the ellipses, the components on their own will not reveal the optimal photon-number-resolving capability of the detector. However, projecting the histogram on an angle of $\alpha = 138^\circ$ [as indicated by the black dashed line in Fig. 3(a)], the maximal photon-number resolution can be unveiled. This projection is required as the principal components describe the maximal variance in the data set, which can be a mixture from various information sources. The projection distills the maximal photon-number resolution from the principal components. This leads to the histogram shown in Fig. 3(b) for a mean photon number of $\bar{n} = 3.5$, where the angle-projected weights are calculated as $w_\alpha = w_2 \sin(\alpha) + w_1 \cos(\alpha)$. After the

angled projection, only one basis function will describe the photon-number dependency. Interpreting this basis function reveals which features of the electrical output trace of an SNSPD need to be observed when it comes to photon-number resolution. We find that the relative time difference between the trigger signal and the rising edge (peak of $-f_\alpha$ around 18 ns in Fig. 2), as well as the peak amplitude of the electrical output signal from the SNSPD (part of $-f_\alpha$ after the peak), contain the most photon-number information.

In a recent study, the relative time difference between a trigger signal and the rising edge as well as the falling edge has been observed in a two-dimensional histogram using a time tagger [29]. In order to compare our oscilloscope measurement (utilizing PCA to show us the best method

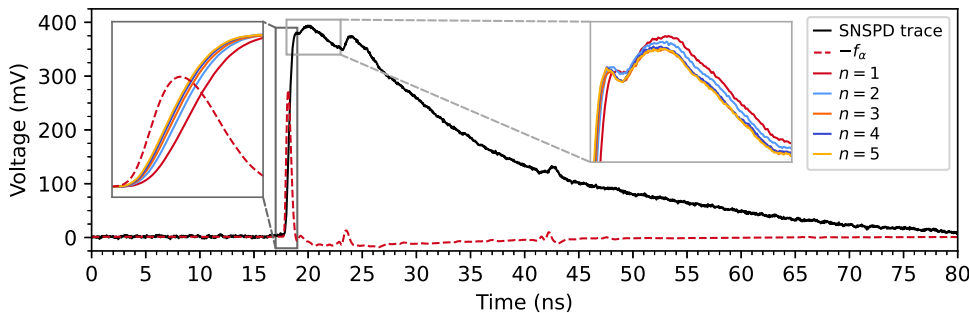


FIG. 4. The electrical output signal of the SNSPD, as well as the angled principal component $-f_\alpha$ (scaled by a factor of 2000 for better comparison). The left inset shows the rising edges of the traces for different photon numbers, where an earlier rising edge correlates with a higher photon number. The right inset shows the peaks of the traces, where a reduced height correlates with a higher photon number. The colors correspond to different photon numbers, as labeled in the legend. For reduced influence of electrical noise, an average over 20 traces is shown for both insets. Features around 24 ns and 43 ns are typically seen for SNSPDs from Single Quantum (see, e.g., Ref. [27]).

to retrieve photon-number information) with the method from Ref. [29], we have also recorded a two-dimensional histogram of the rising and falling edge using a time tagger with a time resolution of < 1.9 ps on the same commercial SNSPD. In the end, this needs less data analysis to show photon-number resolution and is thus more application oriented. We use the same experimental setup shown in Fig. 1, except with a time tagger that records the relative time differences from the trigger signal to the rising and falling edge of the trace. The photon-number resolution depends on the voltage threshold of the time tagger. We find that at half peak height (corresponding to 185 mV), the separation between photon numbers is best. Afterward, we plot the complete data set recorded with the time tagger in a two-dimensional histogram [see Fig. 3(c)], find the optimal projection angle ($\beta = 1.1^\circ$), and plot the distributions for different mean photon numbers [see Fig. 3(d)]. A comparison of the resulting distributions in Figs. 3(b) and 3(d) reveals a very similar performance.

In order to visualize why the two methods lead to similar results, we show an electrical output signal of the SNSPD in Fig. 4 and highlight the key features for photon-number resolution as identified by the PCA. In the insets of Fig. 4, we show an average over 20 SNSPD traces for different photon-number events as identified by the PCA. An increased photon number correlates with a reduced time difference between a trigger signal and the rising edge. This is consistent with previous studies where the rising edge has been observed in order to show photon-number resolution using an SNSPD [21,22,26–29].

In our measurements, an increased photon number correlates with a reduced peak amplitude. This is the opposite of earlier work [21], which has shown an increase in the peak amplitude with the photon number. The difference can be explained with the readout electronics. Reference [21] uses a high-bandwidth amplifier combined with a high-pass filter and therefore amplifies slower signals less

than fast signals. This means that traces corresponding to lower photon numbers are less amplified since they have slower rise times, resulting in a lower peak amplitude. Our readout electronics are a commercial device supplied by the manufacturer of the SNSPD. It is a safe assumption that the amplifier is optimized for signal to noise and thus has a bandwidth closely matching the SNSPD for one-photon detection events. Faster signals are then amplified less, resulting in lower peak amplitudes for multiphoton detection events.

While it is certainly challenging to make simultaneous precise time and voltage measurements, this can be circumvented by only focusing on the time measurement of rising and falling edges using a precise time tagger. The voltage measurement can be converted into a time measurement of the falling edge, since the threshold voltage is at a fixed value. A lower peak amplitude then means an earlier crossing of the threshold voltage. As mentioned above, the threshold of the time tagger needs to be chosen carefully in order to maximize the photon-number resolution. The left inset in Fig. 4 shows that the separation between different photon-number events appears largest at half peak height, which is consistent with the optimized threshold set for the time-tagger measurement.

A comparison of the optimal projection for the PCA in Fig. 3(b) and the time-tagger analysis in Fig. 3(d) shows very close agreement. Due to the increased time resolution of the time tagger, this method is suitable to circumvent the need to measure the peak amplitude of the electrical output signal to optimize the photon-number resolution. In order to characterize the photon-number resolution of the SNSPD, we make use of the confidence measure

$$C_n = \int_{-\infty}^{\infty} \frac{p(w|n)^2 p(n)}{p(w)} dw, \quad (2)$$

which has been proposed by Humphreys *et al.* [31]. This measure describes the probability that a certain detector response yields the correct photon number. Here, $p(n)$ is the probability of an n -photon input, which in our case is a Poissonian distribution. $p(w)$ is the overall probability distribution of the angle-projected weight w_α (angle-projected time w_β) of the two-dimensional histograms in Figs. 3(b) and 3(d). Finally, $p(w|n)$ is the probability $p(w)$ given an incident photon number n . This is derived by fitting Gaussian functions to the individual peaks in the histograms shown in Figs. 3(b) and 3(d). As an example, the distribution $p(w|n=1)$ corresponds to a Gaussian function fitted to the first peak from the right (corresponding to a photon number of $n=1$) to either histogram.

In Fig. 5, we show the confidence C_n for the two data sets (PCA and time-tagger method) for three mean photon numbers. Since this work is focused on the readout of the SNSPD, in Fig. 5 we show the confidence where we do not account for the detector efficiency of $\eta_{\text{det}} = (77 \pm 3)\%$ (nonfaded lines), which means that the confidence only takes into account the correct readout of the photon number absorbed by the SNSPD and not the actual incident photon number. In this way, only the two investigated methods are compared, without the effect of the limited detection efficiency. Taking the nonunity detector efficiency into account reduces the confidence measure, as can be seen by the faded lines in Fig. 5. This is the effect of photon loss, where, e.g., a two-photon event can be caused by a three-photon input, where one photon has been lost, or a four-photon input, where two photons have been lost. When comparing different detectors (and not readout methods), it makes sense to include the detector efficiency when calculating the confidence. However, this work compares readout methods on the same detector. More detail about the calculation of the confidence when including the detector efficiency can be found in Appendix C, where we also show probability distributions $p(w|n)$ and $p(n|w)$. Note that this analysis neglects the effects of dark counts, since these are negligible (10^{-8}) within the detection window. As can be seen in Fig. 3(b) for the PCA data set and in Fig. 3(d) for the time-tagger data set, the photon-number contributions overlap significantly for $n \geq 5$ and $n \geq 6$, respectively. Therefore, we only calculate the confidence up to $n = 4$ (PCA) and $n = 5$ (time tagger). In Fig. 5, we show that the confidence decreases with increasing photon number, which results from the fact that the spacing of the ellipses (corresponding to the photon number) in Figs. 3(a) and 3(c) decreases.

The confidence for the time-tagger measurement is always slightly higher, which can be explained by the higher timing resolution of < 1.9 ps compared to the timing resolution of the oscilloscope of roughly 8 ps. This means that focusing merely on the temporal measurement of the rising and falling edges with a time tagger can effectively substitute measuring the SNSPD

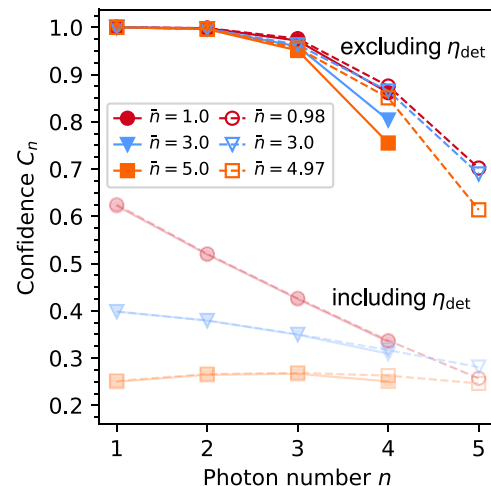


FIG. 5. The confidence C_n versus the photon number for the analysis of the oscilloscope data using PCA (solid symbols and solid lines) and the time-tagger data (hollow symbols and dashed lines) for three mean photon numbers. The nonfaded lines are confidence values excluding the detector efficiency η_{det} and the faded lines are including the detector efficiency. Probability distributions $p(w)$ for the displayed mean photon number are shown in Fig. 3(d) (time-tagger method) and in Fig. 7 (PCA method).

signal amplitude (proposed by the PCA). This makes a time tagger the ideal candidate to extract photon-number information from SNSPDs. Additionally, the width of the ellipses of the time-tagger measurement in Fig. 3(c) is limited by the system jitter of the experimental setup. Reducing the system jitter should therefore improve the photon-number discrimination, more noticeably for higher photon numbers.

IV. CONCLUSIONS

Using PCA (a tool from multivariate statistics) on a set of electrical output signals from an SNSPD allows us to investigate which features of the SNSPD output trace are most relevant for photon-number resolution. Our analysis indicates that the rising edge, as well as the amplitude of the electrical output signal, show the most photon-number information. Thus, simultaneously measuring the rising edge and the amplitude of the SNSPD output signal should maximize the photon-number resolution.

We additionally show that a more application-oriented approach of recording the relative time difference from a trigger signal to the rising and falling edge of the SNSPD output signal in a two-dimensional histogram (recently shown in Ref. [29]) can effectively substitute the voltage measurement by a temporal measurement of the falling edge of the output signal using a time tagger. We explain this by the much better timing resolution of < 1.9 ps of the time tagger compared to the timing resolution of the oscilloscope. We also characterize the photon-number

resolution by calculating a confidence measure [31] (which is the probability that a certain detector response yields the correct photon number) of the two methods presented in this work. We find that the confidence using the time-tagger method is always slightly higher and that the time tagger can in principle resolve higher photon numbers, due to the better timing resolution. This makes the time tagger an excellent tool to enable photon-number resolution with SNSPDs. This method relies on extremely precise timing resolution of the measurement signal, since it is sensitive to the effect of multiple localized breakdowns in superconductivity (“hot spots”) being induced by multiple incident photons. Factors that limit this resolution, primarily system jitter and optical pulse length, will reduce the photon-number-resolving capabilities. It may be possible to modify the detector geometry to increase the optical pulse duration for which this effect persists but this remains an open research question.

The data set of the raw SNSPD traces is freely available at Ref. [33].

ACKNOWLEDGMENTS

We thank Klaus Jöns for lending the oscilloscope and Vladyslav Dyachuk for fruitful discussions. This work was partially funded by the European Union [European Research Council (ERC), “Quantum Engineering of Superconducting Array Detectors In Low-Light Applications” (QuESADILLA), Grant No. 101042399]. The views and opinions expressed are, however, those of the author(s) only and do not necessarily reflect those of the European Union or the European Research Council Executive Agency. Neither the European Union nor the granting authority can be held responsible for them. This work has received funding from the German Ministry of Education

and Research within the PhoQuant project (Grant No. 13N16103).

APPENDIX A: COVARIANCE MATRIX

PCA is a dimensionality-reduction technique. To reduce the complexity of the data set, one first calculates the covariance matrix of the data set. Subsequently, one finds the eigenvectors (principal components in PCA terms) of the largest eigenvalues of the covariance matrix, which correspond to the directions of maximum variance, i.e., information in the data set. The covariance matrix is a square matrix that represents how each data point relates to every other data point. The covariance is a measure of how two data points tend to vary together.

We calculate the covariance matrix of a subset of the full data set, which contains 1000 samples (oscilloscope traces) from each mean photon number (in total, 10^4 samples). Only a small region of the $19\,000 \times 19\,000$ covariance matrix contains relevant entries, which is the region around the rising edge of the electrical output signal of the SNSPD. We show the relevant region of the covariance matrix in Fig. 6(a), together with the first principal component f_1 (white line). It can be seen in Fig. 6(a) that the largest covariance values occur at the rising edge of the electrical output signal of the SNSPD. This indicates that the rising edge causes the most variance (i.e., contains the most information) in the data set. The negative values along the horizontal cut at $y \approx 18.25$ ns (which corresponds to the rising edge) in Fig. 6(a) mean variation in the opposite direction, i.e., increasing values at the rising edge correlate with decreasing values at the falling edge. This is consistent with our findings that an increasing photon number correlates with an earlier rising

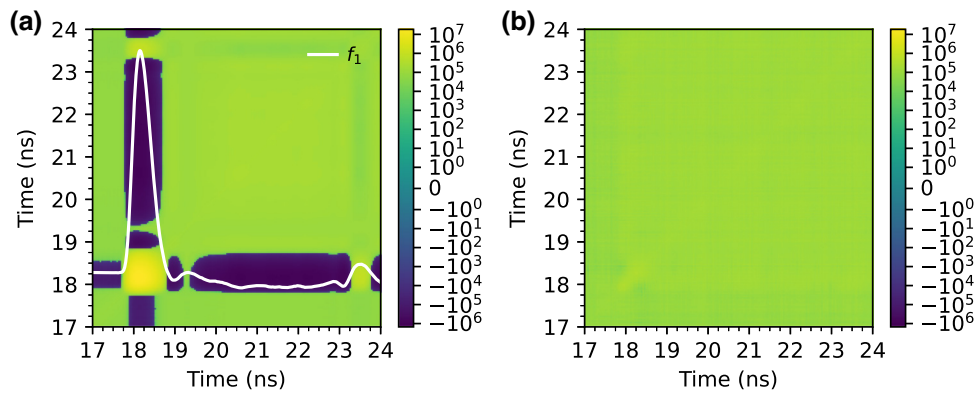


FIG. 6. (a) The covariance matrix of a subset of the full data set [1000 samples (oscilloscope traces) from each mean photon number]. Therefore, this subset contains all photon-number components. The largest (positive) values are around the rising edge of the electrical output signal of the SNSPD. The smallest (negative) values correspond to the falling edge of the signal. The white line (arbitrary scaling) corresponds to the first principal component f_1 (also shown in Fig. 2). f_1 essentially corresponds to the color-axis values of a horizontal cut of the matrix at $y \approx 18.25$ ns. (b) The covariance matrix of 50 samples corresponding to the one-photon component, as identified by the PCA.

edge and a reduced height (or, correspondingly, an earlier falling edge). This behavior is also represented by f_1 , which is the first principal component found by the PCA.

In Fig. 6(b), we show the covariance matrix of 50 samples (oscilloscope traces) corresponding to the one-photon component, as identified by the PCA. This means that we extract only those traces that the PCA has identified as a one-photon event ($n = 1$) and we calculate the covariance matrix based on 50 of these traces. In Fig. 6(b),

it can be seen that there are no relevant contributions to the covariance matrix, which means that all data points vary in the same way. This is expected, as we only use one-photon events, which should produce traces that look very similar and thus have little to no variation between them. When closely examining Fig. 6(b) around the point (18 ns, 18 ns) (which corresponds to the rising edge of the SNSPD traces), slightly larger covariances can be noted. This can be explained by slight variations of the rising edge of the SNSPD traces.

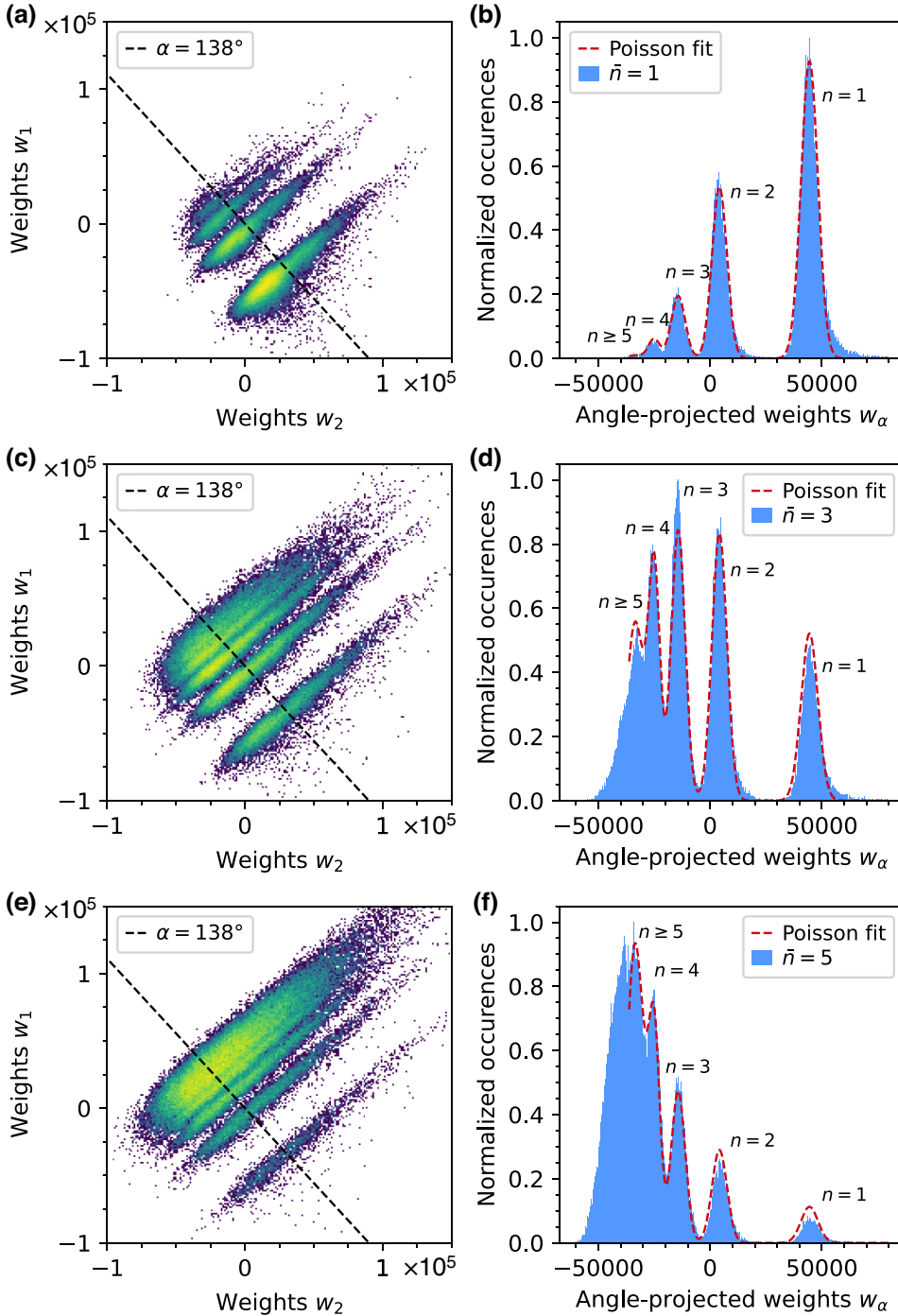


FIG. 7. (a),(c),(e) Two-dimensional histograms of the weights of the first two principal components from the PCA model for mean photon numbers of $\bar{n} = 1$, $\bar{n} = 3$, and $\bar{n} = 5$, respectively. (b),(d),(f) Histograms of the optimal projection at an angle of $\alpha = 138^\circ$ and a multi-Gaussian fit with an enforced Poisson distribution (red dashed line) according to (a), (c), and (e), respectively.

APPENDIX B: PRINCIPAL COMPONENT ANALYSIS

Here, we provide additional two-dimensional histograms from the PCA model, together with their optimal projection at an angle of $\alpha = 138^\circ$, for mean photon numbers of $\bar{n} = 1$, $\bar{n} = 3$ and $\bar{n} = 5$ (see Fig. 7). It can be seen that the occupation of the ellipses shifts toward the upper left of the two-dimensional histograms with increasing mean photon number. These mean photon numbers are used to calculate the confidence in Fig. 5.

APPENDIX C: CONFIDENCE CALCULATION

We characterize the photon-number resolution of the SNSPD using the confidence measure introduced by Humphreys *et al.* [31]:

$$C_n = \int_{-\infty}^{\infty} p(w|n)p(n|w)dw = \int_{-\infty}^{\infty} \frac{p(w|n)^2 p(n)}{p(w)} dw. \quad (\text{C1})$$

Using Bayes' theorem, the confidence can also be expressed using the probabilities $p(w|n)$ and $p(n|w)$, of observing a specific weight w given a photon number n and of observing a specific photon number n given a certain weight w , respectively. To take the limited efficiency of the detector η_{det} into account, the loss matrix

$$L_{n,n'} = \binom{n}{n'} \eta_{\text{det}}^{n'} (1 - \eta_{\text{det}})^{n-n'} \quad (\text{C2})$$

can be used, which is an expression that describes the probability of retaining n' out of n photons including efficiency η_{det} .

In Fig. 8(a), we show $p(w|n)$ as a function of the angle-projected time w_β (for the time-tagger method) for different

photon numbers n . These are (multi-)Gaussian distributions with the mean and standard deviation determined by the underlying probability distribution $p(w)$ [which is the angle-projected histogram shown in Fig. 3(d)]. The amplitudes of the Gaussians are determined by the loss matrix in Eq. (C2), to account for the efficiency of the detector. This is necessary, as it is possible that, e.g., a two-photon event can be caused by a three-photon input, where one photon has been lost, or a four-photon input, where two photons have been lost. In Fig. 8(b), we show $p(n|w)$ for a mean photon number of $\bar{n} = 1$, which can be calculated with Bayes' theorem using $p(w|n)$ [shown in Fig. 8(a)], $p(n)$ (the Poisson distribution for a certain mean photon number \bar{n}), and $p(w)$.

To correctly calculate the confidence, the zero-photon contribution needs to be included as well. Neither the PCA nor the time-tagger method include zero-photon events. Therefore, we use the mean photon-number-dependent closed-form expression for the zero-photon contribution to the confidence,

$$C_{0,\bar{n}} = L_{n,0} \frac{L_{n,0} p(n, \bar{n}')}{p(0, \bar{n})}, \quad (\text{C3})$$

which is then added separately as an additional term to Eq. (C1). Here, $L_{n,0}$ is the probability of losing all n out of n photons given by Eq. (C2), $p(0, \bar{n})$ is the probability of measuring $n = 0$ photons for a mean photon number of \bar{n} (given by a Poisson distribution), and $p(n, \bar{n}')$ is the probability of actually having n photons for a mean photon number of \bar{n}' corrected by the efficiency (also given by a Poisson distribution), i.e., $\bar{n}' = \bar{n}/\eta_{\text{det}}$.

Integrating over the product of the two probability distributions $p(w|n)$ and $p(n|w)$ [shown in Figs. 8(a) and 8(b), respectively] and adding the zero-photon contribution [given by Eq. (C3), when including the detector efficiency η_{det}] for a photon number n and a mean photon number \bar{n}

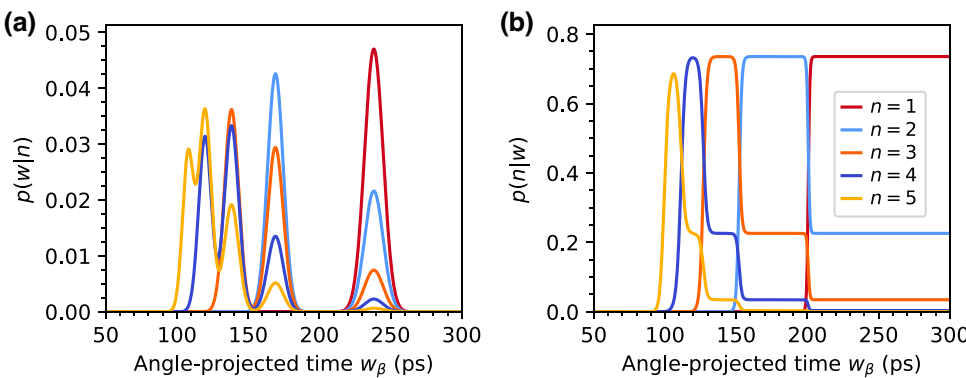


FIG. 8. (a) The probability $p(w|n)$ given an incident photon number n , adjusted for the efficiency of the detector η_{det} . (b) The probability $p(n|w)$ given a certain weight w_β for a mean photon number of $\bar{n} = 1$. These distributions depend on the mean photon number, as they are calculated from $p(w|n)$, $p(w)$ and $p(n)$ using Bayes' theorem.

gives the confidence $C_{n,\bar{n}}$. Confidence values for the PCA method and the time-tagger method are shown in Fig. 5 (including and excluding the detector efficiency η_{det}).

-
- [1] P. Kok, W. J. Munro, K. Nemoto, T. C. Ralph, J. P. Dowling, and G. J. Milburn, Linear optical quantum computing with photonic qubits, *Rev. Mod. Phys.* **79**, 135 (2007).
- [2] N. Gisin, G. Ribordy, W. Tittel, and H. Zbinden, Quantum cryptography, *Rev. Mod. Phys.* **74**, 145 (2002).
- [3] N. Gisin and R. Thew, Quantum communication, *Nat. Photonics* **1**, 165 (2007).
- [4] S. Slussarenko, M. M. Weston, H. M. Chrzanowski, L. K. Shalm, V. B. Verma, S. W. Nam, and G. J. Pryde, Unconditional violation of the shot-noise limit in photonic quantum metrology, *Nat. Photonics* **11**, 700 (2017).
- [5] B. Calkins, A. E. Lita, A. E. Fox, and S. Woo Nam, Faster recovery time of a hot-electron transition-edge sensor by use of normal metal heat-sinks, *Appl. Phys. Lett.* **99**, 241114 (2011).
- [6] H. Paul, P. Törmä, T. Kiss, and I. Jex, Photon chopping: New way to measure the quantum state of light, *Phys. Rev. Lett.* **76**, 2464 (1996).
- [7] D. Achilles, C. Silberhorn, C. Śliwa, K. Banaszek, and I. A. Walmsley, Fiber-assisted detection with photon number resolution, *Opt. Lett.* **28**, 2387 (2003).
- [8] M. J. Fitch, B. C. Jacobs, T. B. Pittman, and J. D. Franson, Photon-number resolution using time-multiplexed single-photon detectors, *Phys. Rev. A* **68**, 43814 (2003).
- [9] K. Banaszek and I. A. Walmsley, Photon counting with a loop detector, *Opt. Lett.* **28**, 52 (2003).
- [10] E. A. Dauler, B. S. Robinson, A. J. Kerman, J. K. W. Yang, K. M. Rosfjord, V. Anant, B. Voronov, G. Gol'tsman, and K. K. Berggren, Multi-element superconducting nanowire single-photon detector, *IEEE Trans. Appl. Supercond.* **17**, 279 (2007).
- [11] R. Cheng, Y. Zhou, S. Wang, M. Shen, T. Taher, and H. X. Tang, A 100-pixel photon-number-resolving detector unveiling photon statistics, *Nat. Photonics* **17**, 112 (2023).
- [12] G. V. Resta, L. Stasi, M. Perrenoud, S. El-Khoury, T. Brydges, R. Thew, H. Zbinden, and F. Bussières, Gigahertz detection rates and dynamic photon-number resolution with superconducting nanowire arrays, *Nano Lett.* **23**, 6018 (2023).
- [13] F. Mattioli, Z. Zhou, A. Gaggero, R. Gaudio, S. Jahanmirnejad, D. Sahin, F. Marsili, R. Leoni, and A. Fiore, Photon-number-resolving superconducting nanowire detectors, *Superconductor Science and Technology* **28**, 104001 (2015).
- [14] J. Huang, W. Zhang, L. You, C. Zhang, C. Lv, Y. Wang, X. Liu, H. Li, and Z. Wang, High speed superconducting nanowire single-photon detector with nine interleaved nanowires, *Supercond. Sci. Technol.* **31**, 74001 (2018).
- [15] W. Zhang, J. Huang, C. Zhang, L. You, C. Lv, L. Zhang, H. Li, Z. Wang, and X. Xie, A 16-pixel interleaved superconducting nanowire single-photon detector array with a maximum count rate exceeding 1.5 GHz, *IEEE Trans. Appl. Supercond.* **29**, 1 (2019).
- [16] G. He, H. Li, R. Yin, L. Zhang, D. Dong, J. Lv, Y. Fei, X. Wang, Q. Chen, F. Li, H. Li, H. Wang, X. Tu, Q. Zhao, X. Jia, J. Chen, L. Kang, and P. Wu, Simultaneous resolution of photon numbers and positions with series-connected superconducting nanowires, *Appl. Phys. Lett.* **120**, 124001 (2022).
- [17] L. Stasi, G. Gras, R. Bertrandouane, M. Perrenoud, H. Zbinden, and F. Bussières, Fast high-efficiency photon-number-resolving parallel superconducting nanowire single-photon detector, *Phys. Rev. Appl.* **19**, 64041 (2023).
- [18] Y. Guan, H. Li, L. Zhang, D. Dong, H. Wang, Q. Chen, S. Guo, B. Zhang, X. Zhang, Z. Yang, X. Tu, Q. Zhao, X. Jia, J. Chen, L. Kang, and P. Wu, Approaching pixel-level readout of SNSPD array by inductor-shaping pulse, *Appl. Phys. Lett.* **123**, 42602 (2023).
- [19] J. Chiles, I. Charaev, R. Lasenby, M. Baryakhtar, J. Huang, A. Roshko, G. Burton, M. Colangelo, K. Van Tilburg, A. Arvanitaki, S. W. Nam, and K. K. Berggren, New constraints on dark photon dark matter with superconducting nanowire detectors in an optical haloscope, *Phys. Rev. Lett.* **128**, 231802 (2022).
- [20] B. Korzh, *et al.*, Demonstration of sub-3 ps temporal resolution with a superconducting nanowire single-photon detector, *Nat. Photonics* **14**, 250 (2020).
- [21] C. Cahall, K. L. Nicolich, N. T. Islam, G. P. Lafyatis, A. J. Miller, D. J. Gauthier, and J. Kim, Multi-photon detection using a conventional superconducting nanowire single-photon detector, *Optica* **4**, 1534 (2017).
- [22] K. L. Nicolich, C. Cahall, N. T. Islam, G. P. Lafyatis, J. Kim, A. J. Miller, and D. J. Gauthier, Universal model for the turn-on dynamics of superconducting nanowire single-photon detectors, *Phys. Rev. Appl.* **12**, 34020 (2019).
- [23] A. J. Kerman, J. K. W. Yang, R. J. Molnar, E. A. Dauler, and K. K. Berggren, Electrothermal feedback in superconducting nanowire single-photon detectors, *Phys. Rev. B* **79**, 100509 (2009).
- [24] D. Zhu, M. Colangelo, C. Chen, B. A. Korzh, F. N. C. Wong, M. D. Shaw, and K. K. Berggren, Resolving photon numbers using a superconducting nanowire with impedance-matching taper, *Nano Lett.* **20**, 3858 (2020).
- [25] M. Bell, A. Antipov, B. Karasik, A. Sergeev, V. Mitin, and A. Verevkin, Photon number-resolved detection with sequentially connected nanowires, *IEEE Trans. Appl. Supercond.* **17**, 289 (2007).
- [26] M. Endo, T. Sonoyama, M. Matsuyama, F. Okamoto, S. Miki, M. Yabuno, F. China, H. Terai, and A. Furusawa, Quantum detector tomography of a superconducting nanostrip photon-number-resolving detector, *Opt. Express* **29**, 11728 (2021).
- [27] S. Sempere-Llagostera, G. S. Thekkadath, R. B. Patel, W. S. Kolthammer, and I. A. Walmsley, Reducing $g^{(2)}(0)$ of a parametric down-conversion source via photon-number resolution with superconducting nanowire detectors, *Opt. Express* **30**, 3138 (2022).
- [28] S. I. Davis, A. Mueller, R. Valivarthi, N. Lauk, L. Narvaez, B. Korzh, A. D. Beyer, O. Cerri, M. Colangelo, K. K. Berggren, M. D. Shaw, S. Xie, N. Sinclair, and M. Spiropulu, Improved heralded single-photon source

- with a photon-number-resolving superconducting nanowire detector, *Phys. Rev. Appl.* **18**, 64007 (2022).
- [29] G. Sauer, M. Kolarczik, R. Gomez, J. Conrad, and F. Steinlechner, Resolving photon numbers using ultra-high-resolution timing of a single low-jitter superconducting nanowire detector, [arXiv:2310.12472](https://arxiv.org/abs/2310.12472) (2023).
- [30] H. Abdi and L. J. Williams, Principal component analysis, *WIREs Comput. Stat.* **2**, 433 (2010).
- [31] P. C. Humphreys, B. J. Metcalf, T. Gerrits, T. Hiemstra, A. E. Lita, J. Nunn, S. W. Nam, A. Datta, W. S. Kolthammer, and I. A. Walmsley, Tomography of photon-number resolv-
- ing continuous-output detectors, *New J. Phys.* **17**, 103044 (2015).
- [32] M. Dryazgov, Y. Korneeva, and A. Korneev, Modeling of distinguishability of nonsimultaneous two-photon events in micron-width superconducting strips, *AIP Conf. Proc.* **2872**, 40001 (2023).
- [33] T. Schapeler, N. Lamberty, T. Hummel, F. Schlue, M. Stefszky, B. Brecht, C. Silberhorn, and T. J. Bartley, SNSPD traces given varying incident mean photon numbers [Data set], Zenodo (2024). <https://doi.org/10.5281/zenodo.10600594>.